Electronic Structures and Optical Properties of Open and Capped Carbon Nanotubes

WanZhen Liang, Xiu Jun Wang, Satoshi Yokojima, and GuanHua Chen*

Contribution from the Department of Chemistry, The University of Hong Kong, Pokfulam Road, Hong Kong

Received February 7, 2000. Revised Manuscript Received August 16, 2000

Abstract: The electronic structures of a series of carbon nanotubes with different sizes, chiralities, ends, and bond lengths are studied systematically. Their absorption spectra are calculated with the localized density matrix method. The semiempirical model PM3 is employed in the calculation. The nature of optical excitations is investigated by examining their reduced single-electron density matrices. It is found that the optical excitations may be divided into the end modes and the tube modes, which have distinctive energies, features, and structural dependences. The optical gaps of carbon nanotubes scale inversely with tube length. Finite optical gaps have been confirmed and determined for infinitely long carbon nanotubes. The densities of states of carbon nanotubes are calculated at the self-consistent Hartree−Fock level. The calculated absorption spectra and densities of states compare well to the experimental results.

I. Introduction

Carbon nanotubes (CNTs) have become an important subject of research activities since their initial finding by Iijima in 1991[1] and the subsequent report of the synthesis of large quantities of CNTs by Ebbesen et al.[2] in 1992. CNTs can be synthesized through carbon arc vaporization in a gas atmosphere or through a transition metal catalytic reaction. The latter method has been used to synthesize single wall nanotubes (SWNTs),[3,4] which may be envisaged as rolled-up graphite sheets. A CNT may be characterized by its chirality, which is denoted by the chiral vector (m,n). Possible applications of the new materials have been reported: as atomic-scale field emitters,[5,6] as pinning materials in high-temperature superconductors,[7] for the tips of scanning tunneling microscopes (STMs),[8−12] as nanowires, as quantum dots,[13] and as electronic rectifiers.[14] CNTs possess very interesting structural and electronic properties. For instance, they have large nonlinear optical responses, and may thus be used for electrooptical devices. The optical properties of CNTs have been investigated,[15−18] and their absorption spectra have been measured.[15,17,18] The optical conductivities of a bundle of SWNTs of 1.3 nm diameter were measured with a low-energy electron energy loss spectrum (EELS) experiment,[16] and interband transitions were seen at 0.65 ± 0.05, 1.2 ± 0.1, 1.8 ± 0.1, 2.4 ± 0.2, 3.1 ± 0.2, 4.3 ± 0.1, and 6.2 ± 0.1 eV. The peak at 0.65 eV is attributed to semiconducting tubes, while the peak at 1.8 eV is attributed to metallic tubes. These are consistent with the STM measurements on metallic tubes.[19] The near-infrared absorption spectra of SWNTs of 1.3 nm diameter and 100−300 nm length are measured, and three peaks at 1.21, 1.14, and 0.67 eV are found. These SWNTs are terminated with chemical functional groups, and the experiment was carried in CS_2 solution.[17,18] Both open-ended and capped CNTs have been observed by high-resolution transmission electron microscope (TEM)[20] and STM[21] techniques. The finite size effect of CNTs has been investigated by Raman spectroscopy, and it has been found that the Raman peaks in the intermediate frequency range are different from those of infinitely long CNTs.[22] The SWNTs and multiwalled carbon nanotubes (MWNTs) have been used as probes in atomic force microscope (AFM).[9] These AFMs have improved lateral resolution and may be applied to biological systems. The CNTs with chemically tailored ends have distinct properties and have been used in chemical force microscope (CFM).[10] For instance, carboxylic acid groups (−COOH) at the open ends of SWNTs were coupled to amines to form probes with hydrophobic functionality. Compared with other tips, CNT tips provide very significant improvements in lateral chemical resolution.[10] SWNTs are the best systems for

* To whom correspondence should be addressed.

(1) Iijima, S. *Nature* **1991**, *354*, 56.
(2) (a) Ebbesen, T. W.; Ajayan, P. M. *Nature* **1992**, *358*, 220. (b) Ebbesen, T. W.; Hiura, H.; Fujita, J.; Ochiai, Y.; Matsui, S.; Tanigaki, K. *Chem. Phys. Lett.* **1993**, *209*, 83.
(3) Iijima S.; Ichihashi, T. *Nature* **1993**, *363*, 603.
(4) Bethune, D. S.; Kiang, C. H.; de Vries, M. S.; Gorman, G.; Savoy, R.; Vazquez, J.; Beyers, R. *Nature* **1993**, *363*, 605.
(5) Rinzler, A. G.; Hafner, J. H.; Nikolaev, P.; Lou, L.; Kim, S. G.; Tománek, D.; Nordlander, P.; Colbert, D. T.; Smalley, R. E. *Science* **1995**, *269*, 1550.
(6) de Heer, W. A.; Châtelain, A.; Ugarte, D. *Science* **1995**, *270*, 1179.
(7) Treacy, M. M. J.; Ebbesen, T. W.; Gibson, J. M. *Nature* **1996**, *381*, 678.
(8) Wong, S. S.; Joselevich, E.; Woolley, A. T.; Cheung, C. L.; Lieber, C. M. *Nature* **1998**, *394*, 52.
(9) Wong, S. S.; Harper, J. D.; Lansbury, P. T., Jr.; Lieber, C. M. *J. Am. Chem. Soc.* **1998**, *120*, 603.
(10) Wong, S. S.; Woolley, A. T.; Joselevich, E.; Cheung, C. L.; Lieber, C. M. *J. Am. Chem. Soc.* **1998**, *120*, 8557.
(11) Hafner, J. H.; Cheung, C. L.; Lieber, C. M. *J. Am. Chem. Soc.* **1999**, *121*, 9750.
(12) Hafner, J. H.; Cheung, C. L.; Lieber, C. M. *Nature* **1999**, *398*, 761.
(13) Sohn, L. L.; Kouwenhoven, L. P.; Schon, G. *Mesoscopic Electron Transport*; Kluwer Academic: Dordrecht, 1997.
(14) Saito, Y.; Uemura, S.; Hamaguchi, K. *Jpn. J. Appl. Phys.* **1998**, *37*, L346.
(15) Liu, X.; Si, J.; Chang, B.; Xu, G.; Yang, Q.; Pan, Z.; Xie, S.; Ye, P.; Fan, J.; Wan, M. *Appl. Phys. Lett.* **1999**, *74*, 164.
(16) Pichler, T.; Kunpfer, M.; Golden, M. S.; Fink, J.; Rinzler, A.; Smalley, R. E. *Phys. Rev. Lett.* **1998**, *80*, 4729.
(17) Chen, J.; Hamon, M. A.; Hu, H.; Chen, Y. S.; Rao, A. M.; Eklund, P. C.; Haddon, R. C. *Science* **1998**, *282*, 95.
(18) Hamon, M. A.; Chen, J.; Hu, H.; Chen, Y. S.; Itkis, M. E.; Rao, A. M.; Eklund, P. C.; Haddon, R. C. *Adv. Mater.* **1999**, *11*, 834.
(19) Wildöer, J. W. G.; Venema, L. C.; Rinzler, A. G.; Smalley, R. E.; Dekker, C. *Nature* **1998**, *391*, 59.
(20) Iijima, S. *Mater. Sci. Eng. B* **1993**, *19*, 172.
(21) Sattler, K. *Carbon* **1995**, *33*, 915.
(22) Saito, R.; Takeya, T.; Kimura, T.; Dresselhaus, G.; Dresselhaus, M. S. *Phys. Rev. B* **1999**, *59*, 2388.

10.1021/ja000469u CCC: $19.00
Published on Web 10/26/2000

investigating intrinsic CNTs' properties because of their structural simplicity. It is predicted that small-diameter nanotubes will exhibit either metallic or semiconducting behavior, depending strongly on tube diameters and chiralities.[23−25] Some of these theoretical predictions have been confirmed experimentally, such as in the STM[26−29] and the EELS[16,30,31] experiments. The density of states (DOS) has been probed directly by STM.[26−28] It has been numerically evaluated by the density functional theory (DFT)[32,33] and tight-binding methods[34−39] as well. The optical spectra of CNTs have been calculated,[40−43] and these calculations were based on Hubbard-like models or were carried at the Hartree−Fock level. More realistic Hamiltonians and better methods which include electron−electron correlation are thus warranted.[11]

Recently, the localized density matrix (LDM) method has been developed to evaluate the ground- and excited-state properties of very large systems.[44−50] It is based on the truncation of reduced single-electron density matrices, and thus, its computation time scales linearly with the system size. The LDM method has been used to determine the absorption spectra of a few open-ended zigzag CNTs.[49] The Pariser−Parr−Pople (PPP) Hamiltonian, which considers merely the π electrons, was employed in the calculation. The curvature of tube leads to the hybridization of π and σ orbitals. The smaller the tube, the more the hybridization. This hybridization may alter significantly the zero-order band structure of small-diameter CNTs as well as the optical properties. Thus, a more realistic model that includes all valence orbitals is needed for CNTs, especially for those with capped ends. Semiempirical methods such as CNDO/S,[51] INDO,[52] MNDO,[53] and AM1[54] consider explicitly all valence electrons. Stewart reparametrized the MNDO Hamiltonian to give an MNDO-PM3 (MNDO parametric method 3) or PM3 Hamiltonian.[55] The PM3 leads to substantially reduced errors for the calculated heat of formation as compared to the MNDO and AM1 methods. It has been employed to evaluate linear and nonlinear optical properties of organic compounds.[56−58]

In this work, the electronic structures of CNTs with different chiralities, ends, and lengths are investigated by the LDM method. The PM3 Hamiltonian is employed in the calculation. π and σ electrons are considered explicitly. Electron−electron correlation is considered within the framework of the time-dependent Hartree−Fock (TDHF) approximation or the random phase approximation (RPA).[59] The optical absorption spectra and DOS are calculated and compared to the experiments. The nature of dipole-induced excitations is determined by examining their reduced density matrices. In section II, a description is given for the implementation of the LDM method at the PM3 level. In section III, the electronic properties of CNTs, such as the absorption spectra and DOS, are calculated and reported, detailed analysis of the excited-state reduced density matrices is carried, and the qualitative nature of these excitations is determined. Finally, discussion and conclusions are given in section IV.

II. The PM3-LDM Method

The PM3 Hamiltonian in the presence of an external field **E** is described as follows,

$$H = H_e + H_{ee} + H_{ext}$$

$$H_e = \sum_{ab}\sum_{mn} H_{ab}^{mn}\, c_{am}^{\dagger} c_{bn}$$

$$H_{ee} = {}^1/_2 \sum_{ab}\sum_{mn,ij} V_{ab}^{mn,ij}\, c_{an}^{\dagger}\, c_{bi}^{\dagger} c_{bj} c_{am}$$

$$H_{ext} = -\mathbf{E}(\mathbf{t})\cdot\hat{\mathbf{P}} \qquad (1)$$

where $c_{am}^{\dagger}$ (c_{bn}) is the creation (annihilation) operator for an electron at a localized atomic orbital m (n) on atom a (b). The one-electron integral H_{ab}^{mn} may be expressed as

$$H_{ab}^{mn} = \langle \chi_a^m | -{}^1/_2\, \nabla_{\mathbf{r}}^2 + U(\mathbf{r}) | \chi_b^n \rangle \qquad (2)$$

where χ_a^m (χ_b^n) is the m (n)-th atomic orbital on atom a (b) and $U(\mathbf{r})$ is the one-electron potential. H_{ee} is the two-electron part of the Hamiltonian which represents the effective electron−electron Coulombic interaction. The PM3 model neglects the differential overlap for atomic orbitals on different atoms; i.e., all of the two-electron integrals are set to zero except for that when the orbitals m and n belong to atom a and i and j belong to atom b. $V_{ab}^{mn,ij}$ is expressed as

(23) Dresselhaus, M. S.; Dresselhaus, G.; Eklund, P. C. *Science of Fullerenes and Carbon Nanotubes*; Academic Press: San Diego, CA, 1996.
(24) (a) Saito, R.; Fujita, M.; Dresselhaus, G.; Dresselhaus, M. S. *Appl. Phys. Lett.* **1992**, *60*, 2204. (b) Saito, R.; Fujita, M.; Dresselhaus, G.; Dresselhaus, M. S. *Phys. Rev. B* **1992**, *46*, 1804.
(25) Saito, R.; Dresselhaus, G.; Dresselhaus, M. S. *Physical Properties of Carbon Nanotubes*; Imperial College Press: London, 1998.
(26) Zhang, Z.; Lieber, C. M. *Appl. Phys. Lett.* **1993**, *62*, 2792.
(27) Odom, T. W.; Huang, J.-L.; Kim P.; Lieber, C. M. *Nature* **1998**, *391*, 62.
(28) Wong, E. W.; Sheehan P. E.; Lieber, C. M. *Science* **1997**, *277*, 1971.
(29) Olk, C. H.; Heremans, J. P. *J. Mater. Res.* **1994**, *9*, 259.
(30) Dravid, V. P.; Lin, X.; Wang, Y.; Wang, X. K.; Yee, A.; Ketterson, J. B.; Chang, R. P. H. *Science* **1993**, *259*, 1601.
(31) Ajayan, P. M.; Iijima, S.; Ichihashi, T. *Phys. Rev. B* **1993**, *47*, 6859.
(32) Rubio, A. *Appl. Phys. A* **1999**, *68*, 275.
(33) Rubio, A.; Sánchez-Portal, D. S.; Artacho, E.; Ordejón, P.; Soler, J. M. *Phys. Rev. Lett.* **1999**, *82*, 3520.
(34) Jishi, R. A.; Bragin, J.; Lou, L. *Phys. Rev. B* **1999**, *59*, 9862.
(35) (a) Charlier, J.-C.; Lambin, P. *Phys. Rev. B* **1998**, *57*, R15037. (b) Charlier, J.-C.; Issi, J.-P. *Appl. Phys. A* **1998**, *67*, 79.
(36) Rochefort, A.; Salahub, D. R.; Avouris, P. *Chem. Phys. Lett.* **1998**, *297*, 45.
(37) Tamura, R.; Tsukada, M. *Phys. Rev. B* **1995**, *52*, 6015.
(38) Chico, L.; Benedict, L. X.; Louie, S. G.; Cohen, M. L. *Phys. Rev. B* **1996**, *54*, 2600.
(39) Rao, A. M.; Richter, E.; Bandow, S.; Chase, B.; Elund, P. C.; Williams, K. A.; Fang, S.; Subbaswamy, K. R.; Menon, M.; Thess, A.; Smalley, R. E.; Dresselhaus, G.; Dresselhaus, M. S. *Science* **1997**, *275*, 187.
(40) Wan, X.; Dong, J.; Xing, D. Y. *Phys. Rev. B* **1998**, *58*, 6756.
(41) Ma, J.; Yuan, R.-K. *Phys. Rev. B* **1998**, *57*, 9343.
(42) Ando, T. *J. Phys. Soc. Jpn.* **1997**, *66*, 1066.
(43) (a) Jiang, J.; Dong J.; Wang, X.; Xing, D. Y. *J. Phys. B* **1998**, *31*, 3079. (b) Jiang, J.; Dong J.; Xing, D. Y. *Phys. Rev. B* **1999**, *59*, 9838.
(44) Yokojima, S.; Chen, G. H. *Chem. Phys. Lett.* **1998**, *292*, 379.
(45) Yokojima, S.; Chen, G. H. *Phys. Rev. B* **1999**, *59*, 7259.
(46) Yokojima, S.; Chen, G. H. *Chem. Phys. Lett.* **1999**, *300*, 540.
(47) Yokojima, S.; Zhou, D. H.; Chen, G. H. *Chem. Phys. Lett.* **1999**, *302*, 495.
(48) Liang, W. Z.; Yokojima, S.; Chen, G. H. *J. Chem. Phys.* **1999**, *110*, 1844.
(49) Liang, W. Z.; Yokojima, S.; Zhou, D. H.; Chen, G. H. *J. Phys. Chem. A* **2000**, *104*, 2445.
(50) Yokojima, S.; Wang, X. J.; Zhou, D. H.; Chen, G. H. *J. Chem. Phys.* **1999**, *111*, 10444.
(51) (a) Del Bene J.; Jaffé, H. H. *J. Chem. Phys.* **1968**, *48*, 1807. (b) Del Bene J.; Jaffé, H. H. *J. Chem. Phys.* **1968**, *48*, 4050.
(52) Pople, J. A.; Beveridge, D. L.; Dobosh, P. A. *J. Chem. Phys.* **1967**, *47*, 2026.
(53) Dewar, M. J. S.; Thiel, W. *J. Am. Chem. Soc.* **1977**, *99*, 4899.
(54) Dewar, M. J. S.; Zoebisch, E. G.; Healy, E. F.; Stewart, J. J. P. *J. Am. Chem. Soc.* **1985**, *107*, 3902.
(55) Stewart, J. J. P. *J. Comput. Chem.* **1989**, *10*, 209.
(56) Duan, X.-M.; Konami, H.; Okada, S.; Oikawa, H.; Matsuda, H.; Nakanishi, H. *J. Phys. Chem.* **1996**, *100*, 17780.
(57) Choi, U. S.; Kim, T. W.; Jung, S. W.; Kim, C. J. *B. Kor. Chem. Soc.* **1998**, *19*, 299.
(58) Matsuzawa, N.; Dixon, D. A. *J. Phys. Chem.* **1992**, *96*, 6232.
(59) Ring, P.; Schuck, P. *The Nuclear Many-Body Problem*; Springer: New York, 1980.

$$V_{ab}^{mn,ij} = \langle \chi_a^n(1)\chi_b^i(2)|V(r_{12})|\chi_a^m(1)\chi_b^j(2)\rangle \quad (3)$$

H_{ext} is the interaction between the valence electrons and an external electric field $\boldsymbol{E}(t)$, and $\hat{\mathbf{P}}$ is the molecular dipole moment operator. As a consequence, the Fock matrix h may be written as

$$h_{ab}^{mn} = H_{ab}^{mn} + 2\delta_{ab}\sum_c\sum_{ij\in c} V_{ac}^{mn,ij}\rho_{cc}^{ij} - \sum_{i\in a}\sum_{j\in b} V_{ab}^{mi,jn}\rho_{ab}^{ij} \quad (4)$$

Similarly, the induced Fock matrix may be expressed as follows,

$$\delta h_{ab}^{mn} = 2\delta_{ab}\sum_c\sum_{ij\in c} V_{ac}^{mn,ij}\delta\rho_{cc}^{ij} - \sum_{i\in a}\sum_{j\in b} V_{ab}^{mi,jn}\delta\rho_{ab}^{ij} \quad (5)$$

The operator for DOS can be defined as

$$\hat{\rho} = \sum_m |m\rangle\langle m|\delta(E - E_m) \quad (6)$$

where $|m\rangle$ is the state m, and E_m is its energy. The DOS of a system is then given by[60]

$$\sum_m \delta(E - E_m) = Tr\hat{\rho}(E)$$

$$= \frac{1}{\pi}\mathrm{Im}\sum_m \lim_{\eta\to 0^-}\frac{1}{E - E_m - i\eta} \quad (7)$$

If the $|m\rangle$ is a Hartree−Fock (HF) molecular orbital, eq 7 gives the one-electron DOS.

III. Results of Calculation

A. Absorption Spectra of Carbon Nanotubes. To test the validity of the PM3 model for determining optical spectroscopy, we calculate the absorption spectrum of a C_{60} molecule. The result is demonstrated in Figure 1. The geometry optimization for C_{60} is carried out at the Hartree−Fock level using the PM3 Hamiltonian. The calculated energies of the first three main absorption peaks in C_{60} are 3.8, 4.6, and 5.7 eV, which compare well to the corresponding experimental values of 3.7, 4.6, and 5.7 eV for C_{60} in *n*-hexane solution.[61] The calculations are carried out using our LDM program with inclusion of all reduced single-electron density matrix elements (i.e., full TDHF calculation).

A series of CNTs with different chiralities and ends are investigated, and their absorption spectra are determined. The external field is polarized along the tube axis in all calculations. Most CNTs' geometries are optimized at the Hartree−Fock level, except for those specified otherwise in the text. In our calculations, open-ended CNTs are terminated with hydrogen atoms or other functional groups. Capped CNTs are closed with fullerene-like cages which contain only hexagonal and pentagonal faces. For instance, a C_{60} molecule is bisected at its equator, and two resulting half-spheres may be attached to an open-ended (5,5) armchair tube or (9,0) zigzag tube, depending on the way that the C_{60} molecule is cut. Six pentagons are needed to form a cap for a (5,0) tube, and six pentagons together with one hexagon are needed for a (6,0) tube, since a total of 12 pentagons are needed to form a closed polygon, which is required by Euler's theorem and sp^2 hybridization.

The influence of two ends upon the optical properties of CNTs is examined. The calculated absorption spectra are shown in Figure 1 for (9,0) CNTs of the same length but different ends.

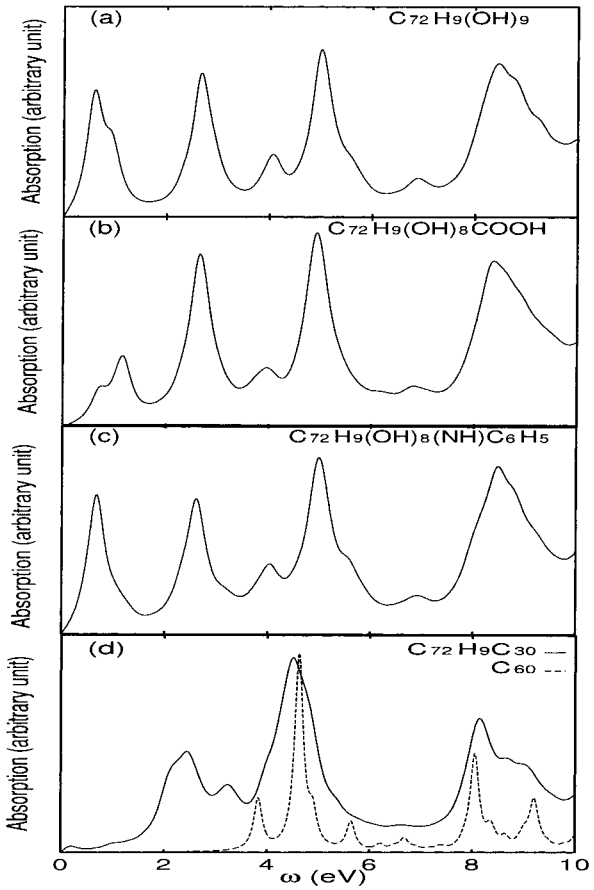

Figure 1. Calculated absorption spectra of C_{60} with dephasing parameter $\gamma = 0.1$ eV and the (9,0) CNTs with $\gamma = 0.2$ eV. Spectra a−d are the absorption spectra for $C_{72}(H)_9(OH)_9$, $C_{72}(H)_9(OH)_8(COOH)$, $C_{72}(H)_9(OH)_8(NH)(C_6H_5)$, and $C_{72+39}H_9$ obtained by using the full TDHF method, respectively. All the geometries are optimized at the HF level with the PM3 Hamiltonian.

Figure 1a−d shows the spectra of $C_{72}H_9(OH)_9$ (one end with −OH and another end with hydrogens), $C_{72}(OH)_8H_9(COOH)$ (one −OH is replaced by −COOH), $C_{72}(OH)_8H_9(NH)C_6H_5$, (one −OH is replaced by $-(NH)C_6H_5$), and $C_{72+30}H_9$ (one end with caps, another end with hydrogens), respectively. Similar line shapes are observed for $\omega > 2.0$ eV in all spectra. The peaks centered at about 2.7, 4.0, 5.0, 6.9, and 8.0 eV are observed in all systems and are attributed to the excitations along the tubes. They are not significantly influenced by the different terminating functional groups. Differences appear at $\omega < 2.0$ eV, which should correspond to the excitations at two tube ends. The HOMOs and LUMOs of CNTs have large components at the ends. This is further verified by the density matrices of low-energy excitations.

The physical properties of infinite CNTs are determined by their chiralities and radii.[22,24,26−28] For finite size tubes, we find that the tube length also plays a vital role in the electronic structure. Figures 2 and 3 are the calculated absorption spectra of different size (9,0) and (5,5) CNTs. Figure 2 shows the absorption spectra of capped (9,0) CNTs. As the number of carbon atoms increases from 78 to 222 (Figure 2a−d), the peaks at $\omega < 6.0$ eV red-shift, while those around 8.0 eV change little. As a consequence of the red-shift, the line shapes differ for $\omega < 6.0$ eV until saturation is reached. The absorption spectra of open-ended (9,0) tubes differ drastically from those of capped (9,0) CNTs, especially when the tube lengths are short. The peaks at low energy ($\omega < 2.0$ eV) for $C_{72}H_9(OH)_9$ (Figure 1a) disappear in the absorption spectrum of C_{72+60} (Figure 2c). The

(60) Li, M. F. *Modern Semiconductor Quantum Physics*; World Scientific: Singapore: 1995.

(61) Leach, S.; Vervloet, M.; Despres, A.; Breheret, E.; Hare, J. P.; Dennis, T. J.; Kroto, H. W.; Taylor, R.; Walton, D. R. M. *Chem. Phys.* **1992**, *160*, 451.

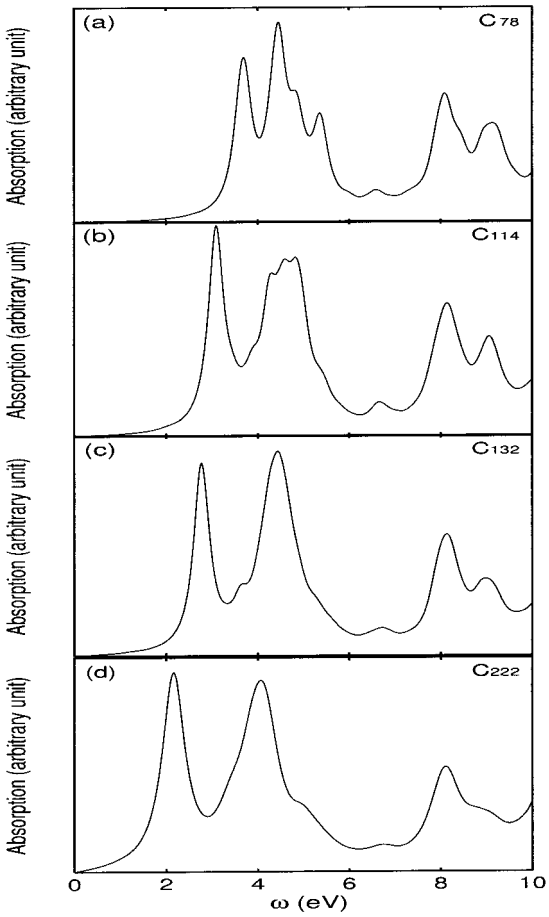

Figure 2. Absorption spectra of capped (9,0) tubes calculated by using the full TDHF and LDM methods. Spectra a−c are the results calculated by using the full TDHF method with $\gamma = 0.2$ eV, and spectrum d is the result obtained by using the LDM method with $\gamma = 0.3$ eV. All of the geometries are optimized.

absorption spectrum of open-ended (9,0) tubes changes drastically with increasing size. The first two peaks of $C_{72}H_9(OH)_9$ disappear when the number of carbon atoms increases to 162, while the third peak shifts below 2.0 eV. Investigation of the corresponding density matrices reveals that the first peak for $C_{72}H_9(OH)_9$ corresponds to the electron−hole pairs located at the two ends. The two ends play an important role in the optical response of short, open-ended zigzag tubes, and their influence diminishes as the size increases. Absorption spectra of several SWNTs with different end groups have been measured, and little variance in the spectra has been observed.[18] This is consistent with our finding that the end groups of long SWNTs have little effect on their absorption spectra. The absorption spectra of (5,5) CNTs (see Figure 3) are similar to those of capped (9,0) CNTs. This is because both tubes have similar radii (3.5 Å for (9,0) and 3.4 Å for (5,5)). The tight-binding calculations have predicted similar electronic and optical behavior for (5,5) and (9,0) tubes.[23] The optical absorption spectra of capped and open-ended (5,5) look similar. For instance, a mere small red-shift is observed for the open-ended (5,5) tube $C_{90}H_{20}$ (solid line in Figure 3e) as compared to the capped C_{90+60} tube (Figure 3c) of the same cylindrical length.

The energy of first major peak (or optical gap) of capped (9,0) and (5,5) CNTs versus $1/N$ is plotted in Figure 4, where N is the number of carbon atoms. The two dashed lines are the linear fits and are almost identical. The optical gaps approach $E_g = 1.23$ eV as the sizes of both tubes approach infinity. Since the radii of the two CNTs are similar, the resulting optical gaps

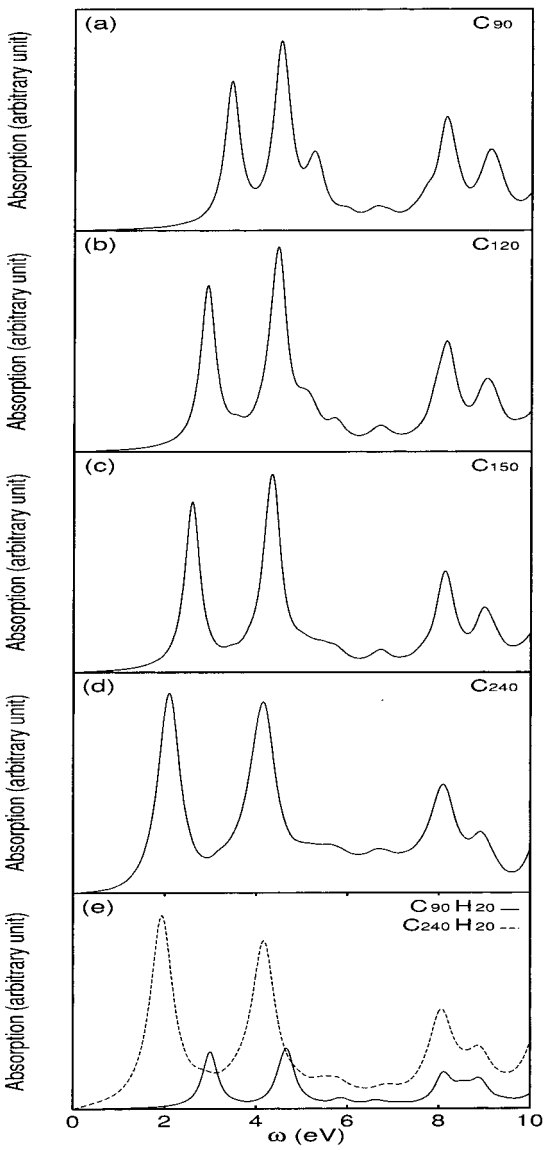

Figure 3. Absorption spectra of open-ended and capped (5,5) armchair tubes calculated by using the full TDHF and LDM methods. Spectra a−d are the absorption spectra of the capped (5,5) tubes. Spectrum e is the absorption spectra of the open-ended (5,5) tubes. The solid line is for $C_{10j}H_{20}$ ($j = 9$), and the dashed line is for $j = 24$. Spectra a−c and e (solid line) were calculated with $\gamma = 0.2$ eV, while $\gamma = 0.3$ eV was employed in the calculation of spectra d and e (dashed line). All of the geometries are optimized.

for two infinitely long tubes have the same values up to the second decimal digits. It may be generalized that the optical gaps for infinitely long tubes are finite and their values depend mainly on the tube radii. The optical absorption spectra of finite size capped (9,0) and (5,5) CNTs have been calculated by using the tight-binding model with only π orbitals of carbon atoms considered. The tight-binding optical gaps for the (9,0) tube with $N = 420$ and the (5,5) tube with $N = 250$ are 1.2 and 1.25 eV, respectively.[41,43] These are comparable to our optical gaps for infinitely long CNTs. The optical signal at ∼1.2 eV has been observed in the optical conductivity and absorption measurement of SWNTs.[16,17] In addition, a gap of 1.2 eV has been observed in the calculated DOS spectrum for (9,0) by the tight-binding method.[23]

The absorption spectra of capped (5,0) tubes with $N = 150$ and 250 and of the (6,0) tube with $N = 156$ and 252 are shown in Figure 5. The absorption spectra of (5,0) with $N = 150$ and

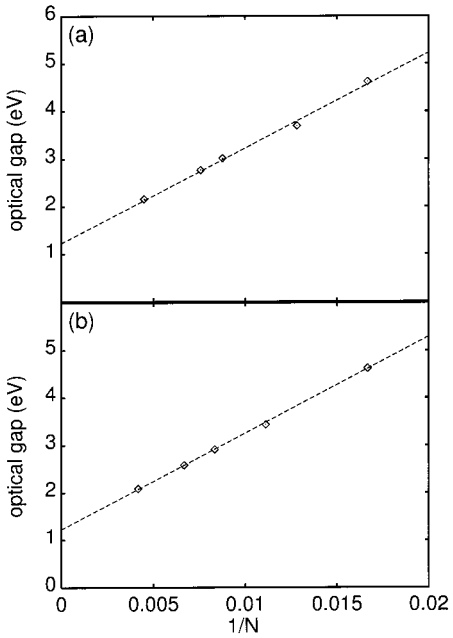

Figure 4. Optical gap via 1/*N* for the capped (9,0) (a) and (5,5) (b) tubes.

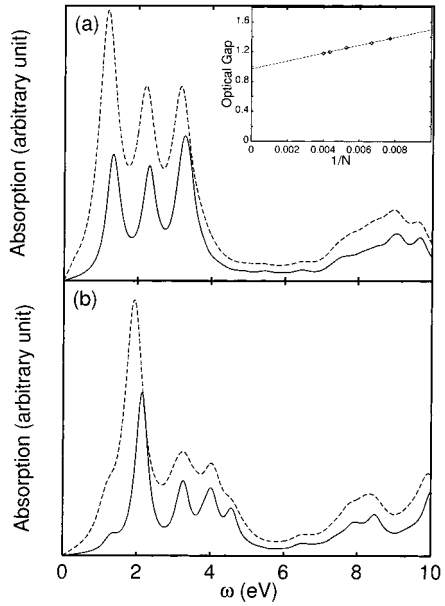

Figure 5. Absorption spectra of the capped (5,0) and (6,0) tubes. (a) The absorption spectra of (5,0) C_{150} (solid line) and C_{250} (dashed line) calculated by using the full TDHF and LDM methods with dephasing $\gamma = 0.2$ and 0.3 eV, respectively. The inset shows the optical gap via 1/*N* for the (5,0) tube. (b) The absorption spectra of the capped (6,0) tube. The solid line is for C_{156} calculated by using the full TDHF method with $\gamma = 0.2$ eV. The dashed line is for C_{252} calculated by using the LDM method with dephasing $\gamma = 0.3$ eV. All of the geometries are optimized.

(6,0) with $N = 156$ are calculated by using the full TDHF method with the dephasing coefficient $\gamma = 0.2$ eV. The absorption spectra of two other tubes are calculated by using the LDM method with $\gamma = 0.3$ eV and a cutoff distance $l_0 = l_1 = 29$ Å. As expected, the red-shifts occur when the system sizes increase. The optical gap of the infinite (5,0) tube approaches ~1.0 eV, as shown in the inset of Figure 5a. A much weaker peak appears at $\omega \approx 1.4$ eV for the (6,0) tube. This is because the optimized geometry for the (6,0) tube has C_{2v} point group symmetry, which is different from the C_{3h} point group symmetry

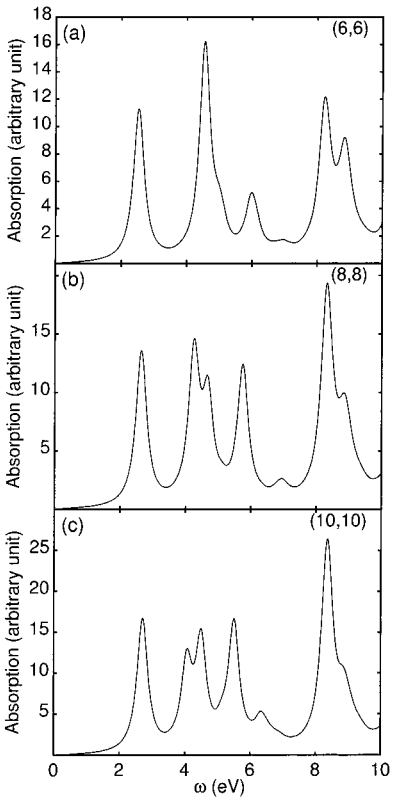

Figure 6. Absorption spectra of the (*m*,*m*) armchair tube with $m = 6$, 8, and 10 and dephasing $\gamma = 0.2$ eV. The ideal structure is employed. (a) The absorption spectra of (6,6) $C_{12j}H_{24}$. (b) The absorption spectra of (8,8) $C_{16j}H_{32}$. (c) The absorption spectra of (10,10) $C_{20j}H_{40}$, with $j = 8$.

of the (9,0) tube. Tubes such as (9,0) and (5,5) have the first major absorption peak located at a larger transition energy, while (5,0) tubes of the same length possess relatively small optical gaps. This suggests that the geometry plays a fundamental role in determining the optical behavior of CNTs.

A broad group of peaks located at 6.0−7.0 eV is observed in the absorption spectra of capped (5,0), (6,0), (9,0), and (5,5) tubes. These peaks shift little as the tube lengths increase and are identified mainly as $\pi-\pi^*$ transitions by the low-energy EELS experiments[16] and calculations.[62] The relative oscillator strength decreases with decreasing tube radius. This is caused by larger $\pi-\sigma$ hybridization in smaller radius tubes. The larger the curvature, the more the π and σ hybridization.

Figure 6 shows the optical absorption spectra of open-ended armchair tubes ($C_{4mj}H_{2m}$) with $j = 4$ and $m = 6$, 8, and 10. The ideal structures, which are rolled up from a single graphite sheet with all bond lengths set to 1.421 Å, are adopted here. The absorption spectra red-shift as the tube radius increases, with the exception of the first peak, which blue-shifts slightly. The blue-shift may result from the competition between the size effect and π orbital overlapping. When the external electric field is applied perpendicular to the tube axis, red-shifts of the lowest peaks are observed when the radii of tubes increase. This is consistent with the expectation that the lowest peak red-shifts as the radius increases (see Figure 7, where the optical gap versus 1/*r* is plotted, with *r* being the radius of the tube). A linear relationship between the gap and 1/*r* is observed, and a gap of 0.7 eV is determined as $r \rightarrow \infty$. It is also found that the

(62) (a) Lin, M.-F.; Shung, K. W.-K. *Phys. Rev. B* **1994**, *50*, 17744. (b) Lin, M.-F.; Shung, K. W.-K.; Chuu, D. S.; Huang C. S.; Lin Y. K. *Phys. Rev. B* **1996**, *53*, 15493.

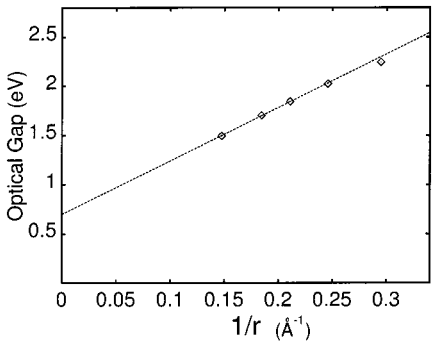

Figure 7. Optical gap via $1/r$ when the external field is applied perpendicular to the tube axis.

absorption threshold is significantly higher for the external field polarized along the tube axis compared to that perpendicular to the tube axis. The absorption spectra of (6,6), (8,8), and (10,-10) are very different from that of (5,5) (solid line in Figure 3e). This is because different bond lengths are used here. Thus, it is concluded that the nature of the excitations is sensitive to the bond lengths. The density matrices in molecular orbital (MO) representation reveal that the first peak in armchair tubes result mainly from the HOMO $\rightarrow$ LUMO + 1 and HOMO $-$ 1 $\rightarrow$ LUMO transitions. The HOMO $\rightarrow$ LUMO transition is forbidden. The other peaks red-shift with increasing tube radius. The relative oscillator strengths of these peaks, which center at relatively high energy (from 4.3 to 8.2 eV), increase with increasing radius. These peaks correspond to $\pi-\pi^*$ and small-fraction $\pi-\sigma^*$ transitions.

B. Density Matrices of Dipole-Induced Excitations. To understand the nature of electronic excitations, the induced density matrices $\delta\rho^{(1)}(\omega)$ of $C_{72}H_9(OH)_9$ are examined at 0.61, 2.67, and 5.01 eV, those of C_{72+60} at 2.77, 6.72, and 8.14 eV, and those of $C_{80}H_{20}$ at 2.89, 4.79, and 8.04 eV. $C_{72}H_9(OH)_9$ and C_{72+60} are open-ended and capped (9,0) tubes, respectively, and $C_{80}H_{20}$ is an open-ended (5,5) tube. The results are shown in the Figures 8$-$10. The atomic orbital (AO) representation is employed. The atomic indices are assigned increasingly from one end of tube to another, and the orbital indices are arranged in the order of 2s, $2p_x$, $2p_y$, and $2p_z$. The absolute values of density matrix elements are shown in the contour plots. A logarithmic scale is employed. The scales employed for ground- and excited-state density matrices are shown in Figure 8e and f, respectively. From the contour plots in Figures 8a, 9a, and 10a, it is observed that the ground-state density matrices of the three systems are almost diagonal. However, the electron coherence between the two ends is strong in the open-ended (9,0) tube compared to that in the capped (9,0) and (5,5) CNTs. The strong electron coherence between the two open ends of (9,0) has a significant influence on the optical properties. The excited-state density matrices are obtained by the Fourier transformation

$$\delta\rho(\omega) = \int \mathrm{d}t\, \mathrm{e}^{i\omega t}\delta\rho(t) \qquad (8)$$

In the actual TDHF calculation, dephasing γ is added to calculate the time evolution of $\delta\rho(t)$. $\delta\rho(\omega)$ contains not only the effect of the mode at ω but also the effect of other modes. When γ is much lower than the energy differences between different excitations, mixing of other excitations in $\delta\rho(\omega)$ ($\omega \sim \Omega_\nu$) is negligible. Therefore, $\mathrm{Im}[\delta\rho(\Omega_\nu)]$ is a very good approximation for the reduced density matrix for the excitation at Ω_ν. The density matrices shown below take the form $(\mathrm{Im}(\delta\rho(\omega)) + \mathrm{Im}(\delta\rho^{\mathrm{T}}(\omega)))/(i2^{1/2})$, where $\delta\rho^{\mathrm{T}}(\omega)$ is the transpose of $\delta\rho(\omega)$. Three excited-state density matrices of the open-ended (9,0) tube are shown in Figure 8b$-$d. The first excitation at $\omega = 0.61$ eV in $C_{72}H_9(OH)_9$ includes mostly the π electron$-$hole pairs from the two ends. This peak disappears in the absorption spectra of capped (9,0) tubes. The contribution from the electron$-$hole pairs among the π orbitals located in the middle of tube increases for the excitation at $\omega = 2.67$ eV. The excitation at 5.01 eV in $C_{72}H_9(OH)_9$ contains π as well as σ orbital contributions. In general, a contribution from the electron$-$hole pairs in the middle increases rapidly as energy increases. As expected, the oscillator strengths of these excitations increase and their energies red-shift with increasing sizes.[49]

Figure 9b$-$d depict the excited-state density matrices of the capped (9,0) tube C_{72+60} at energies of 2.77, 6.72, and 8.14 eV, while Figure 10b$-$d show the excited-state density matrices of the open-ended (5,5) tube at energies of 2.89, 4.79, and 8.04 eV, respectively. The contributions from the two ends are much weaker compared to that of $C_{72}H_9(OH)_9$; i.e., the electron coherence between the two ends is weak. The main contributions are from the middle of the tubes. This is the reason why the absorption spectra are rather similar for (5,5) and capped (9,0) tubes. The peaks centered at the low energies of 2.77 eV in Figure 9b and 2.89 and 4.79 eV in Figure 10b and c result mostly from π electron$-$hole pairs. The first peak in both systems results mostly from HOMO $\rightarrow$ LUMO + 1 and HOMO $-$ 1 $\rightarrow$ LUMO transitions. HOMO $\rightarrow$ LUMO + 2 and HOMO $-$ 2 $\rightarrow$ LUMO also contribute significantly to the first peak ($\omega = 2.77$ eV) of the capped (9,0) tube. Other transitions between the HOMO $-$ m and LUMO + n also contribute to the first peaks of the (9,0) and (5,5) tubes. The white squares in Figure 9b correspond to the electron coherence between two orbitals which belong to two atoms located respectively at the n-th ring and the $(n \pm j)$-th rings, where j is a positive odd number. The antidiagonal part is nearly zero in Figures 9b and 10b. The white square in the antidiagonal part corresponds to the elements between the two orbitals which belong to the two atoms located respectively at two mirror rings which are symmetric with respect to the middle plane. Their values are almost zero except for the pairs of π orbitals which belong to two mirror symmetric atoms. The σ electrons have a larger contribution in the high-energy range—for instance, the peaks at 6.72 and 8.14 eV (Figure 9c,d) in the capped (9,0) tube and the peak at 8.04 eV (Figure 10d) in the (5,5) tube. These peaks originate from the main $\pi-\pi^*$ transition as well as the partial $\pi-\sigma^*$ transition, and this is revealed by the corresponding density matrices in the MO representation. These excitations have been observed by using the low-energy EELS experiment.[31] The electron coherence among $\pi-\pi^*$ has larger spatial extents than those of $\pi-\sigma^*$, $\sigma-\pi^*$, and $\sigma-\sigma^*$ (see Figure 9c,d). Examining the excited-state density matrices of these three systems reveals that π orbitals are mainly responsible for electron excitations with $\omega < 8.0$ eV, while σ electron are responsible for higher energy electron excitations. The patterns of reduced density matrix contour plots reflect the structure features of CNTs. For instance, the stripes in Figures 8a,d, 9a,c,d, and 10a,c,d are the manifestation of underlying ring structure of CNTs. The "chess board" pattern in Figure 9b reflects large electron coherence among the same ring or between adjacent rings (the dark squares) and diminishing electron coherence between adjacent or next-nearest adjacent rings.

C. Density of States. The scanning tunneling microscope (STM) may probe directly one electron orbital density or DOS. Figure 11 shows the DOS of several CNTs, $C_{300}H_{20}$, $C_{316}H_{20}$, and $C_{320}H_{20}$. The chiralities of these three CNTs are (6,4), (7,3),

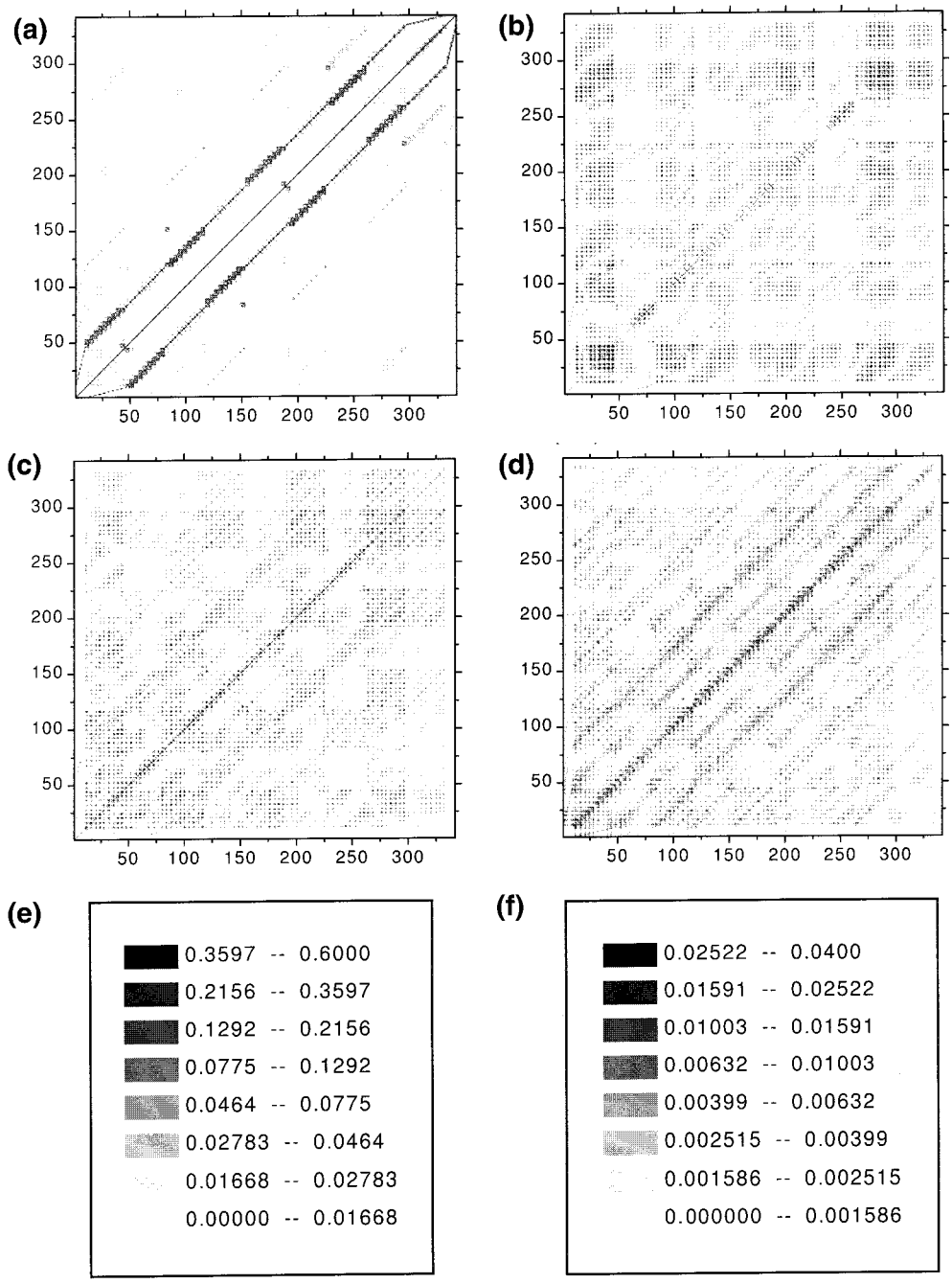

Figure 8. Density matrices of ground states and various excited states for the open-ended (9,0) $C_{72}H_9(OH)_9$ tube in AO representation, calculated by using the full TDHF with $\gamma = 0.1$ eV. The absolute value of the matrix elements is shown by a gray logarithmic scale. (a) The density matrix of the ground state. (b) $\omega = 0.61$ eV. (c) $\omega = 2.67$ eV. (d) $\omega = 5.01$ eV. (e) The scale of all of the ground-state density matrices. (f) The scale of all of the excited states.

and (5,5), respectively. The ideal structures are employed. Their radii are 3.415, 3.482, and 3.393 Å, and their lengths are 35.3, 34.91, and 38.14 Å, respectively. The Fermi energy level is between the HOMO and LUMO and is set to zero. According to the tight-binding model, a CNT with chirality (m,n) is a conductor when $m - n = 3I$ (I is a integer). A CNT with other chiralities is a semiconductor. Our calculation shows that the HOMO−LUMO gap for a (5,5) is 2.8 eV, while (7,3) and (6,4) have much smaller gaps although the three radii and lengths are of similar values. The DOS spectra are determined by the CNTs' chiralities. Further, we find that the HOMO−LUMO energy difference decreases overall as the nanotube length increases, and the energy gap in the DOS spectrum may be different from the HOMO−LUMO energy difference. This energy gap and the DOS spectrum saturate when the length is long enough. Our calculated HOMO−LUMO energy gap of the (5,5) tubes is larger than that of the tight-binding calculation for CNTs of the same length since the HOMO−LUMO energy gaps predicted by the tight-binding calculation saturate more rapidly than those by predicted by ab initio HF or semiempirical methods.[63] It is worth pointing out that the DOS of the (5,5) tubes calculated by using the tight-binding model is similar in appearance to our result, and a gap of 2.0 eV exists. However, its value between the gap is small but finite. Our calculated DOS is not symmetric with respect to the Fermi level. This is

(63) Rochefort, A.; Salahub, D. R.; Avouris, P. *J. Phys. Chem. B* **1999**, *103*, 641.

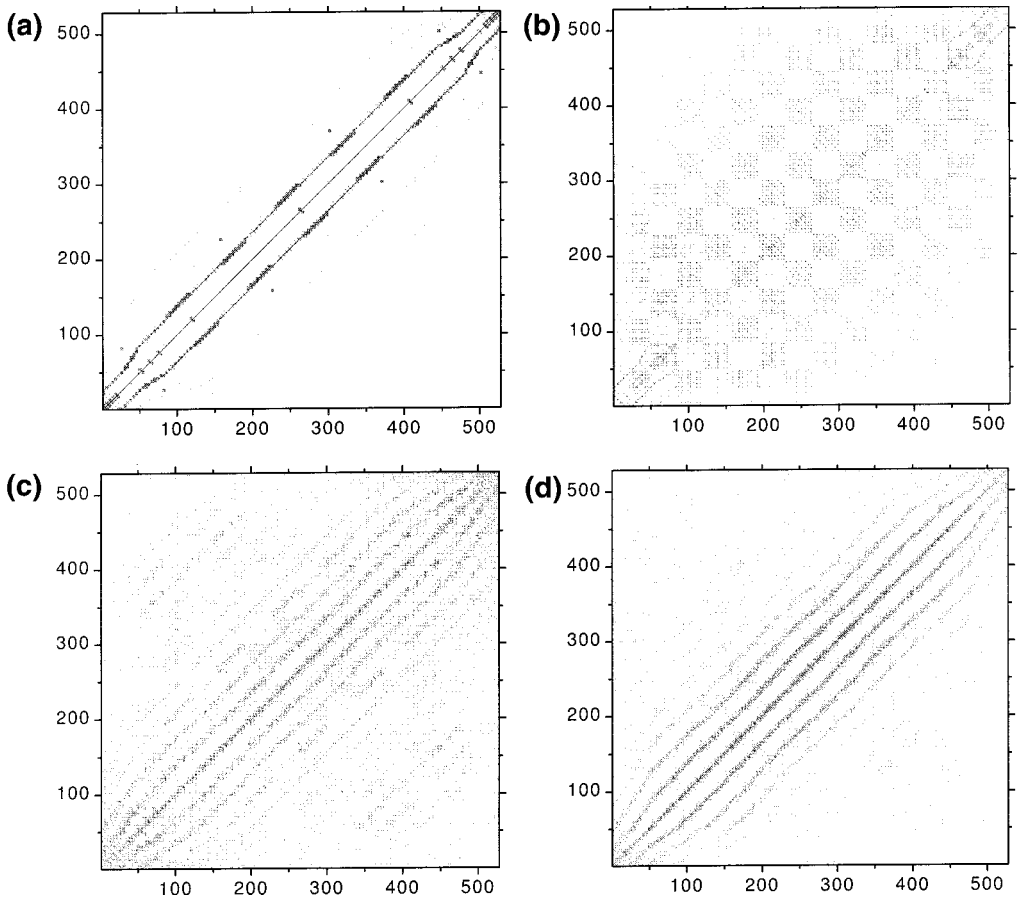

Figure 9. Density matrices of ground states and various excited states for the capped (9,0) tube C_{132} in AO representation, calculated by using the full TDHF method with $\gamma = 0.1$ eV. (a) The density matrix of the ground state. (b) $\omega = 2.77$ eV. (c) $\omega = 6.72$ eV. (d) $\omega = 8.14$ eV.

consistent with the experiment[64] but differs from the tight-binding results.[35,36,39] The difference stems from $\pi-\sigma$ hybridization.[65]

IV. Conclusion

The absorption spectra of a series of CNTs with different sizes, chiralities, ends, and bond lengths are calculated by using the LDM method and the PM3 Hamiltonian. The dipole-induced excitations may be categorized into the end modes (low energy) and the tube modes (high energy). These modes have been characterized by examining their reduced single-electron density matrices. It is found that the optical properties are strongly affected by the tube length, radius, end group, and chirality as well as the bond length. The density matrices of various excitations exhibit interesting features which are related to the structural features of CNTs. The main results are summarized as follows.

(1) The low-energy dipole-induced excitations that appear in the absorption spectra in Figure 1 are the end modes, i.e., the electron−hole pairs that reside mostly at the two ends of tube. These excitations result mainly from $\pi-\pi^*$ transitions. The corresponding absorption peaks have been observed only for short, open-ended zigzag CNTs in our calculations. The excitation energy and oscillator strength depend sensitively on the tube length, ends, and chirality. As the length increases, the low-energy ($\omega \leq 1.0$ eV) absorption peaks red-shift and the oscillator strengths decrease. When the end groups are altered, the profile of the low-energy absorption spectra changes drastically for short CNTs. Their sensitivities to the end groups may be used to design new SWNT-based materials. It is interesting to note that the capped zigzag CNTs and armchair tubes do not have such low-energy absorption peaks. We emphasize that the absorption spectra of long SWNTs appear differently and are affected little by the caps or end groups. This has been confirmed experimentally.[18]

(2) For $\omega \geq 2.0$ eV in Figure 1, the dipole-induced excitations are regarded as the tube modes, i.e., the electron−hole pairs residing in the middle of tube. The energies and oscillator strengths of these tube modes may depend on the tube lengths, radii, and bond length alternations. However, they are not sensitive to the chirality and end groups. It is emphasized that the absorption spectra for capped (9,0), capped (5,5), and open-ended (5,5) tubes of the same length are strikingly similar.

(3) The tube modes may be divided further into two groups of excitations: $2.0 \leq \omega \leq 6.0$ eV and $\omega \geq 6.0$ eV. For the excitations whose energies ω are between 2.0 and 6.0 eV, the electron−hole pairs arise from $\pi-\pi^*$ transitions. These excitations are sensitive to the tube length. As the tube length increases, the corresponding absorption peaks red-shift (see Figures 1−5). The absorption spectrum saturates when the tube length reaches a few nanometers. The calculated optical gaps are consistent with the energy gaps measured by the STM experiment.[16] When the radii increase, most absorption peaks in the range $2.0 \leq \omega \leq 6.0$ eV red-shift, except for the first absorption peaks of armchair CNTs (see Figure 6), which blue-shift slightly when the external field is polarized along the tube. This may be explained on the basis of the competing effects between the hopping matrix elements of π electrons and the tube radii.

(64) Kim, P.; Odom, T. W.; Huang, J.-L.; Lieber, C. M. *Phys. Rev. Lett.* **1999**, *82*, 1225.

(65) Blase, X.; Benedict, L. X.; Shirley, E. L.; Louie, S. G. *Phys. Rev. Lett.* **1994**, *72*, 1878.

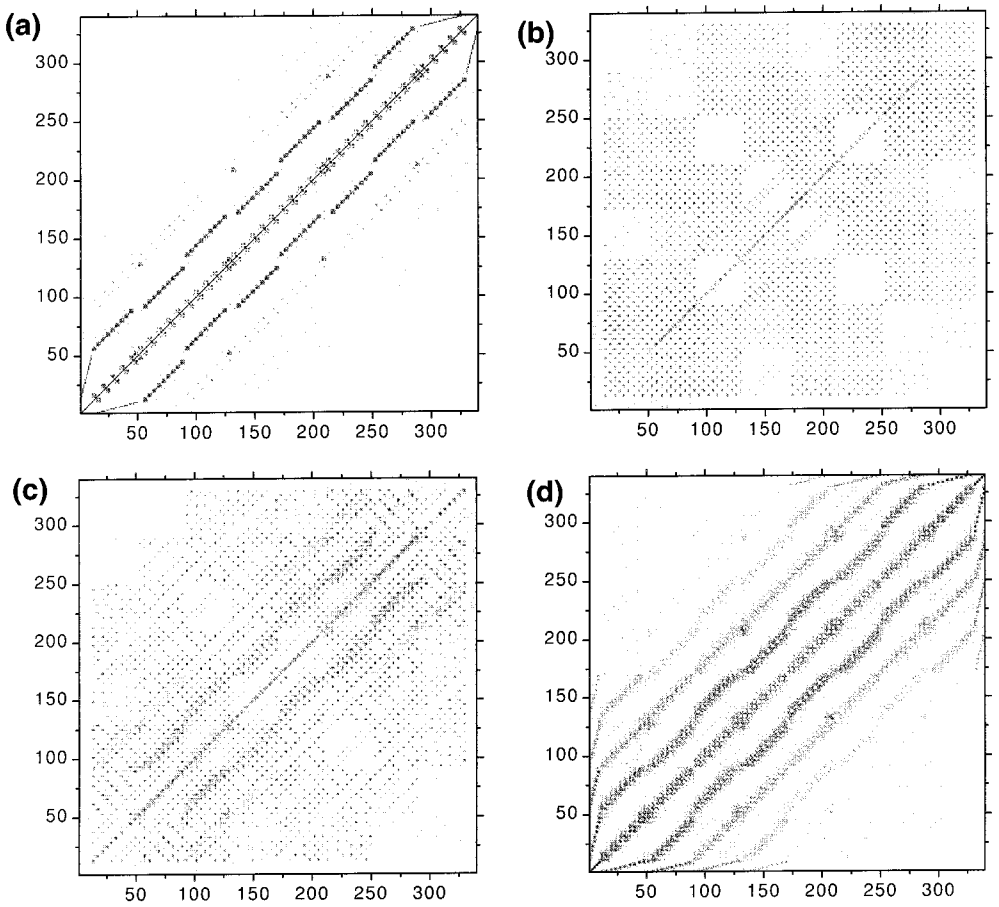

Figure 10. Density matrices of ground states and various excited states for the open-ended (5,5) tube $C_{80}H_{20}$ in AO representation, calculated by using the full TDHF with $\gamma = 0.1$ eV. (a) The density matrix of the ground state. (b) $\omega = 2.89$ eV. (c) $\omega = 4.79$ eV. (d) $\omega = 8.04$ eV.

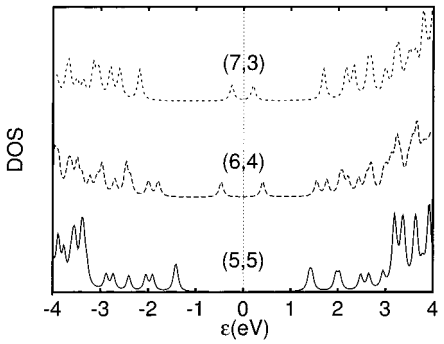

Figure 11. DOS of HF molecular orbitals of (5,5) $C_{320}H_{20}$, (7,3) $C_{312}H_{20}$, and (6,4) $C_{300}H_{20}$, calculated by using the PM3 Hamiltonian. The Fermi level is set to $\epsilon = 0.0$ eV. The energy resolution $\eta = 0.05$ eV is employed.

(4) For the dipole-induced excitations with $\omega \geq 6.0$ eV, their energies and oscillator strengths are not sensitive to the length, chirality, and ends. But the oscillator strengths are sensitive to the tube radii and bond length alternation. The broad peaks at 6.0−7.0 eV and 8.0−9.0 eV are mostly from the $\pi-\pi^*$ transitions, but a small fraction of $\pi-\sigma^*$, $\sigma-\pi^*$, and $\sigma-\sigma^*$ transitions also contribute to these peaks.

(5) For the open-ended tubes containing a few hundred atoms, it is observed that the HOMO−LUMO gaps for armchair CNTs are quite large (∼2.0 eV for (5,5)). This confirms the earlier ab initio Hartree−Fock and semiempirical calculations.[63] It was postulated that this larger HOMO−LUMO gap is due to the finite size effect. As the tube length increases to infinity, the gap may saturate to zero. Our calculation shows evidence for such a postulation.

(6) Finally, the optical gaps of CNTs are finite and approach nonzero values as the tube lengths approach infinity. It is illustrated that the optical gaps depend linearly on $1/N$. The inverse dependence of the optical gap on diameter has been investigated in armchair tube (m,m). It is found that the optical gaps depend inversely on the diameter of the tubes when the external electric field is applied perpendicular to the tube axis.

In summary, the dipole-induced excitations may be categorized into the end modes and tube modes. The end modes are sensitive to the tube length, chirality, and radius in addition to the bond length. When the tube length becomes long enough or the ends are closed with carbon cages, the corresponding low-energy absorption peaks disappear. The tube modes are of higher energy and are less sensitive to the tube length and chirality. The dipole-induced transitions below 8.0 eV are composed mainly of $\pi-\pi^*$ transitions. Further, it has been found that the optical gap scales linearly with $1/N$ and is finite when the number of carbon atoms N approaches infinity. Although the precise values of excitation energies and oscillator strengths may depend on detailed structures of CNTs, the above qualitative conclusion on composition and categorization of CNTs' optical excitations remains valid.

Acknowledgment. We thank Mr. Man Fai Ng for providing the CNTs structures. Support from the Hong Kong Research Grant Council (RGC) and the Committee for Research and Conference Grants (CRCG) of the University of Hong Kong is gratefully acknowledged.

JA000469U